

Magnetic correlation effects by the topological zero mode in a hydrogenated graphene vacancy V_{111}

Naoki Morishita,^{*} Gagus Ketut Sunnardianto,[†] and Koichi Kusakabe[‡]
*Graduate School of Engineering Science, Osaka University,
1-3 Machikaneyama-cho, Toyonaka, Osaka, 560-8531 Japan.*

Isao Maruyama
*Faculty of Information Engineering, Fukuoka Institute of Technology,
3-30-1 Wajiro, Higashi, Higashi-ku, Fukuoka, 811-0295, Japan.*

Kazuyuki Takai
*Faculty of Bioscience and Applied Chemistry, Hosei University,
3-7-2 Kajinocho, Koganei, Tokyo, 184-8584, Japan.*

Toshiaki Enoki
*Department of Chemistry, Tokyo Institute of Technology,
2-12-1 Ookayama, Meguro-ku, Tokyo, 152-8551, Japan.*
(Dated: December 31, 2014)

Electron correlation effects caused by the topological zero mode of a hydrogenated graphene vacancy, V_{111} , with three adsorbed hydrogen atoms is discussed theoretically. A Kondo model is derived from the multi-reference representation of the density functional theory, where exchange scattering processes between the zero mode and low-energy modes in the Dirac cones are estimated. Even when the Dirac cone is slightly off from the charge neutral point, a finite on-site correlation energy, U_0 , for the zero mode of an isolated V_{111} allows the half-filling of the localized level giving a spin $s = 1/2$. The anti-ferromagnetic Kondo screening mediated by higher order scattering processes becomes dominant in the dilute limit of the vacancies. Our estimation of relevant two body interactions certifies appearance of the Kondo effect at low temperatures.

I. INTRODUCTION

After the finding of graphene and its unique properties,[1–3] there has been a lot of discussions on possible electronic correlation effects in various defects of graphene. In theory, correlation effects in defect-induced magnetism were treated by applying several types of models.[4–7] Actually, the Kondo effect in graphene was highlighted for magnetic adatoms.[8–16] Furthermore, vacancy induced magnetism was focused after experimental findings were announced,[17–21] for which the Kondo effect was discussed theoretically.[6, 22–24] Theoretical analysis of possible defective graphene structures has been continuously performed, where hydrogenation of an atomic vacancy was analyzed by theoretical simulations.[17, 25–27]

Recently, identification of hydrogenated graphene vacancies (HGV) was successfully performed utilizing the high-resolution scanning tunneling microscopy supported by electronic structure calculations based on the density functional theory.[28, 29] This experimental result revives researchers' attention to HGV, among various defect structures of graphene.[1, 4] Atomic hydrogen treatment after Ar^+ irradiation on a crystalline graphitic sam-

ple is indeed an important method to create various types of defects including hydrogenated atomic vacancy and nano-holes in a controlled manner.

In the experiment,[28] two stable HGV structures, called V_{111} and V_{211} , were identified. The former, which is a triply hydrogenated atomic vacancy, possesses a topological localized state, *i.e.* the zero mode, according to the local topological network of the π electron system. While, the latter quadruply hydrogenated atomic vacancy does not have the zero mode. Therefore, the former structure of V_{111} may have a localized spin $s = 1/2$. Furthermore, electron correlation effects including the Kondo effect may be expected, similar to the bare vacancy.

The zero-energy non-bonding localized state appears owing to topological characteristic of the π network around V_{111} . Namely, around the vacancy, the number of the B sublattice, N_B , is locally less than that of the A sublattice, N_A , owing to the vacancy, assuming that the original graphene has balanced sublattices. In the argument of network topology of the π system, the difference of $N_A - N_B = 1$ certifies appearance of the π -non-bonding state at the Dirac point. These features of the special localized electron mode are completely reproduced in the band structure calculations. The simulated STM image is almost perfectly identical to the real observation, where usage of the deformed atomic structure optimized by the simulation is essential. Thus, the zero mode localized around the V_{111} structure is confirmed

^{*} morishi@artemis.mp.es.osaka-u.ac.jp

[†] gagus@artemis.mp.es.osaka-u.ac.jp

[‡] kabe@mp.es.osaka-u.ac.jp

both in experiment and by theory.[28]

The location of the zero mode of V_{111} along the energy axis is at the Dirac point. This is always the case, when we simulate a neutral graphene with the triply hydrogenated atomic vacancy. In this condition, the occupation of the zero mode is just at the half-filling. Therefore, a magnetic moment of $s = 1/2$ may appear in the real system, as a Kramers doublet. The correlation effect should be relevant for the magnetic property of V_{111} , which may give an isolated magnetic impurity. To confirm this picture, therefore, we need to go one step further beyond a single-particle description of the ordinary density functional theory (DFT).

In this communication, we propose a method to model the correlated electron system of V_{111} . By evaluating the single-particle spectrum and two-particle effective scattering amplitudes, we derive a kind of the s - d exchange model[30] or a Kondo Hamiltonian[31] describing the action of the zero mode appearing in the hydrogenated graphene vacancy. The Kohn-Sham orbitals obtained by the local density approximation[32] are used to estimate the scattering amplitudes. Here, relevant two-body interactions include the on-site repulsive interaction on the zero mode and effective exchange scatterings between the zero mode and the Dirac electrons.

Converting the exchange operator into a separable form, we obtain an effective Anderson model with two local orbitals. Applying the continuous-time quantum Monte-Carlo calculation, we estimate the chemical potential dependence of the electron number on these local orbitals. The result suggests that the Kondo screening of the spin $1/2$ at the zero mode can happen. In our representation, low-lying orbitals in the Dirac cones are correlated with the zero mode, forming a local singlet pair in the thermodynamic limit. This is a result of magnetic screening mediated by a kind of anti-ferromagnetic super exchange. However, the total ground state remains to be a doublet, which appears as a half-filled renormalized spectrum of the Dirac cones. The state should keep the zero-gap semiconducting feature of the graphene.

II. MODELS OF THE ZERO MODE ON V_{111}

A. The zero mode

At the triply hydrogenated vacancy, each hydrogen atom of V_{111} forms a σ bond with a carbon atom. We have perfect termination of carbon σ dangling bonds at this vacancy. All of the carbon atoms have saturated σ bonds, and there is a π orbital at each carbon atom.

Here, lobes of the π orbital is oriented in a direction nearly perpendicular to the local sp^2 σ bonds. To describe a basic idea on the π topology, at first, we neglect the deformation of graphene sheet around V_{111} . By drawing connections between neighboring π orbitals, we have a honeycomb network with a vacancy. (Fig. 1)

To avoid effects of graphene edges, we may use the

periodic boundary condition along two in-plane directions. The structure contains N_C carbon atoms and three hydrogen atoms. The carbon network gives a bipartite graph, where all vertices are grouped in one of two subsets, A or B , such that two neighboring carbons connected by an edge are contained in the other subsets, *i.e.* one in A and the other in B . Owing to the vacancy site, which is in the B sublattice, the number of A sublattice sites is larger than that of B sublattice sites by 1, *i.e.* $N_A - N_B = 1$. We have $N_C = N_A + N_B$.

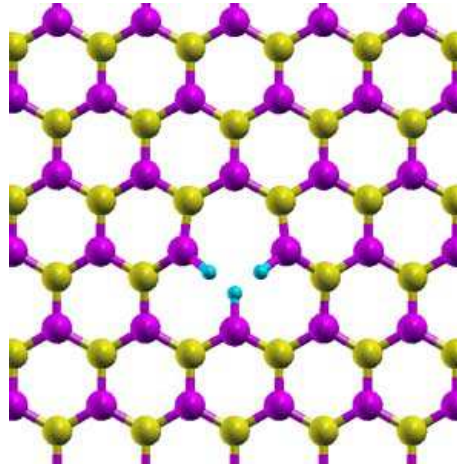


FIG. 1. The atomic structure of V_{111} . Carbon atoms are grouped into subsets, A and B , where atoms in A and B are colored magenta and yellow, respectively. Hydrogen atoms are in cyan. At each carbon site, we have a π orbital. The connections, each of which links two neighboring carbon atoms in a pair, give a defective honeycomb network of V_{111} . This drawing is created by using XCrySDen.[33]

When we adopt a scheme of tight-binding description for a pure π system, assuming that transfer parameters are nearly the same and are non-zero only for each neighboring pair of carbon sites, we have a tight-binding model, *i.e.* the t only model. Introducing the creation (and annihilation) operators, $C_{i,\sigma}^\dagger$ ($C_{i,\sigma}$), of a π electron at the i -th carbon site, we have a Hamiltonian operator of the t model,

$$\begin{aligned} \hat{H}_{TBM} &= -t \sum_{\langle i,j \rangle} \sum_{\sigma=\uparrow,\downarrow} \left\{ C_{i,\sigma}^\dagger C_{j,\sigma} + H.c. \right\} \\ &= \sum_{\sigma=\uparrow,\downarrow} \left(C_{i_A,\sigma}^\dagger, C_{j_B,\sigma}^\dagger \right) H_{TBM} \begin{pmatrix} C_{i_A,\sigma} \\ C_{j_B,\sigma} \end{pmatrix} \\ &= \sum_{k=-N_B}^{N_B} \sum_{\sigma=\uparrow,\downarrow} \tilde{\epsilon}_k C_{k,\sigma}^\dagger c_{k,\sigma}, \\ H_{TBM} &= \begin{pmatrix} 0 & H_{AB} \\ H_{BA} & 0 \end{pmatrix}. \end{aligned} \quad (1)$$

Here, a symbol of $\langle i,j \rangle$ is used to specify a summation with respect to the neighboring pair of carbon atoms. In

the above expression of \hat{H}_{TBM} , the diagonal representation by $c_{k,\sigma}^\dagger$ and $c_{k,\sigma}$ is given by the unitary transformation to perform the diagonalization of H_{TBM} . The eigen energy, $\tilde{\epsilon}_k$, gives the spectrum of the t model on the honeycomb network with a vacancy.

Here, the matrix H_{TBM} is an $(N_C \times N_C)$ matrix with an $(N_A \times N_B)$ submatrix H_{AB} representing hopping processes from a B site to an A site. The index i_A (or j_B) runs only in the A (or B) sublattice sites and $(C_{i_A,\sigma}^\dagger, C_{j_B,\sigma}^\dagger)$ is treated as a $(1 \times N_C)$ vector form. The matrix H_{TBM} has $(N_A \times N_A)$ and $(N_B \times N_B)$ zero matrices as its diagonal submatrices, which represents the bipartiteness leading us to a particle-hole symmetry. The quasi spinor representation allows us to have a gauge transformation,

$$C_{i_A,\sigma}^\dagger \longrightarrow d_{i_A,\sigma}, \quad C_{j_B,\sigma}^\dagger \longrightarrow (-1) \times d_{j_B,\sigma},$$

which gives

$$\begin{aligned} \hat{H}_{TBM} &= \sum_{\sigma=\uparrow,\downarrow} \left(d_{i_A,\sigma}^\dagger, d_{j_B,\sigma}^\dagger \right) H_{TBM} \begin{pmatrix} d_{i_A,\sigma} \\ d_{j_B,\sigma} \end{pmatrix} \\ &= -t \sum_{\langle i,j \rangle} \sum_{\sigma=\uparrow,\downarrow} \left\{ d_{i,\sigma}^\dagger d_{j,\sigma} + H.c. \right\}, \end{aligned} \quad (2)$$

so that the spectrum of the hole Hamiltonian is the same as the original. With a single vacancy in the honeycomb network, $N_A - N_B = 1$, since the rank of the matrix H_{TBM} is no more than $2N_B = N_A + N_B - 1 = N_C - 1$, a conclusion is that a zero eigen value appears at the center of the spectrum. This argument is well known.[34] Furthermore, when the spectrum of H_{TBM} has a discrete nature, the zero eigen mode is stable against perturbation. In its diagonal form, the spectrum of \hat{H}_{TBM} , $\tilde{\epsilon}_k$, is specified by an integer, $-N_B \leq k \leq N_B$. IN the t model, $\tilde{\epsilon}_{-k} = -\tilde{\epsilon}_k$ owing to the particle-hole symmetry. The $k = 0$ mode is the zero mode with $\tilde{\epsilon}_0 = 0$.

This zero mode of the t model was analyzed in its nature as a non-bonding damping mode.[5] In that study, the authors considered a t - t' model with a one-dimensional boundary condition of a semi-infinite system. The spectrum they considered was continuous at the Dirac point, where the upper and lower continuum in the spectrum touched the zero mode peak in a local density of state. When the particle-hole symmetry is broken, the zero mode became a resonance mode.

Let's consider a supercell structure of N_C carbon atoms of V_{111} in a unit cell. We assume that there are N_{cell} supercells as a whole, adopting the Born-von-Karman periodic boundary condition. For the t model, owing to the unbalanced sublattice structures, the total system has $N_{cell} \times (N_A - N_B)$ zero modes. These zero modes provide an exactly flat band for the t model.

Owing to a finite size of the cell, a gap at the Dirac point can be formed. As for the t model, we may make a choice of the supercell in a rhomboid form with $N_C = 2 \times (3n \pm 1)^2 - 1$. Here, n is an integer. We will call the cell a $(3n \pm 1) \times (3n \pm 1)$ cell. On this system, the band

structure shows a gap at the K and K' points of the folded Brillouin zone (FBZ). The flat band appears as ingap states. (For comparison with the DFT simulation, see also Appendix A.) In this model V_{111} structure, we expect stability of the flat band against small perturbation. As for the other $3n \times 3n$ supercell with $N_C = 2 \times (3n)^2 - 1$, the flat band touches the Dirac cones at the Γ point. This is owing to an adjusted periodicity of Bloch wave functions at K (or K'), which allows one of recombined Dirac-cone branches unaffected by the defect.

Similarly, we might have a nearly flat band in a generalized tight-binding model of V_{111} , where long-range transfer terms, s and p orbitals are considered. Using a parameter sets of Papaconstantopoulos with additional parameters for C-H σ bonds,[35, 36] we have obtained band structures for V_{111} . In the actual V_{111} structure, we have slight corrugation of graphene plane around the vacancy. This is due to the geometric exclusion among hydrogen atoms coming from the inter-atomic interaction. Therefore, for the calculation of the s - p model, we utilize an atomic structure obtained by an optimization simulation in a DFT-Kohn-Sham local-density-approximation (LDA) scheme.[32, 37] The obtained band structures are roughly similar to that of the t model. When we see supercells of $n = 3, 4$, we have always a nearly flat band at the Fermi level,

The similarity in the band structures suggests that we have a mapping from an eigen state of the s - p model to a counterpart of the t model, at least when the eigen modes around the Fermi level are concerned. The $(N_C + 1)/2 + (3N_C + 3)/2$ -th band of the s - p model may be a correspondence to the $(N_C + 1)/2$ -th band of the t model. Here, for a definition of the mapping, a π orbital at each carbon site is required. Actually, it is possible to define a local π orbital in the deformed graphene structure of V_{111} . (See a method in Appendix B.) Then, our whole simulations suggest that there is a well-defined topological mapping between an s - p model and the t model as far as V_{111} in a finite cell structure with the periodic boundary condition is considered.

The mapping among low-lying phase spaces of different effective models allows us to call the low-lying flat band "the zero modes". When we take the limit of large supercell size, or $N_C \rightarrow \infty$, the true relevance of the idea will appear. Before going to this point, let us introduce the DFT simulation and another effective many-body Hamiltonian.

B. Scaling of effective Hamiltonians

All of reported band structure calculations of V_{111} in a super cell, based on the density functional theory, told that a flat band appears around the Dirac point.[27, 28] In this band, each eigen state of the Kohn-Sham Hamiltonian has a non-bonding character, where the wave function has a finite amplitude at every A -site carbon atom. This flat band is made from a localized mode around the

vacancy in each cell.

We have obtained the band structures by the DFT-LDA model for $(3n \pm 1) \times (3n \pm 1)$ super cells with $n = 2, 3, 4$ as well as $3n \times 3n$ cells with $n = 2, 3, 4$. Always, we see the flat band, whose dispersion is essentially the same as the previous results. (Appendix A) Interestingly, around the Fermi energy, the dispersion relation in the DFT-LDA modeling is always well reproduced by the s - p tight-binding model. On an above mentioned finite size cell, we know that the s - p model has a mapping to the t model. Therefore, the flat-band mode coming from the pure topological origin of the π network is identified as the zero mode. This is a reason for the terminology, which has already been used in Section I, and is a key for the next discussion.

In an actual calculation with a $3n \times 3n$ super cell, hybridization between the Dirac mode and the zero mode appears significantly at the Γ point of FBZ. However, even in this supercell, the flat band keeps its identity, when we choose the k point apart from the Γ point. Furthermore, there is a gap at the Dirac point for $(3n \pm 1) \times (3n \pm 1)$ supercells, at least when $n < O(10)$. (Appendix A) Then, it is allowable to identify the flat band as zero modes in a finite-sized cell.

When we consider mapping among single-particle eigen states, we use effective single-particle descriptions. In this representation, the zero mode might become a resonance in general, especially in the thermodynamic limit. For a test, we performed a finite-size scaling analysis of the flat band both in DFT and the s - p tight-binding model. (See the DFT results in Appendix A.) Actually, the flat band is shown to be merged in the lower branches of the Dirac cone in the large cell size limit, when we adopt a linear scaling of the energy as a function of $1/n$ within a selected series of $(3n + 1) \times (3n + 1)$. The other series should show a similar behavior, when they are properly analyzed. (See also Appendix C.)

To have the good definition of the zero mode, in a thermodynamic limit, we adopt the next strategy. The strong correlation effect is taken into account in each finite-sized system, before approaching the limit. Having a well-identified correlated eigen state in an effective many-body model, we can have the limit by certifying identity of the correlated ground state of HGV. Thus, we consider a many-body model to describe correlation effects created by the special non-bonding damping mode, *i.e.* the zero mode.

Here, we should comment on the eigen wavefunctions, $\psi_l(\mathbf{r})$, of a single-particle part of the Hamiltonian. Using the set of $\{\psi_l(\mathbf{r})\}$ as an expanding basis, we have a full description of the many-body Hamiltonian. There, any unitary transformation among the basis does not change the final answer. We may make a good choice of the basis set to have a well-converged description. Therefore, we consider a representation obtained in a finite super cell to construct the scaling and the limit.

The electron occupation of the zero mode in the many-body ground state is the second key. Let us consider

neutral systems. For a finite super cell considered, the flat band is half-filled in DFT or TBMs. Furthermore, if we consider a cell with only one V_{111} structure in the periodic boundary condition, one zero mode appears to be just half-filled. Namely, one electron occupies a single zero mode at the Fermi level in the non-interacting particle picture.

Once the zero mode goes into a continuum of the Dirac modes, and if we consider the electron occupation in a free-particle picture, the zero mode has to be off from the half-filling. We should have a finite amplitude of the double occupation of the zero mode effectively in the electronic state, which implies that the correlation between two electrons occupying the zero mode becomes non negligible. Therefore, we have to consider the correlation effect carefully in the thermodynamic limit. To keep away from the energy increment by a finite amount of the double occupation amplitude of the localized mode, we need to take the large cell size limit, keeping identity of the zero mode from the continuum of the Dirac-cone modes.

To have a description of the local electron correlation in a DFT model, the Wannier transformation with the local projection operators is often applied.[38–40] This method derives a mapping from the branches around the Fermi level of the DFT-LDA model to a tight-binding model. When the number of low-lying modes are selected to be the same, relevant eigen modes around the Fermi level are mapped to the corresponding modes of a simplified model, except for high-energy band crossing points.

In the Wannier-transformation scheme, to have the complete expanding basis of the π system, every local π orbital, $\phi_i(\mathbf{r})$, on the i -th carbon atom has to appear in the transformed representation. The size and the shape of $\phi_i(\mathbf{r})$ is almost the same, irrespective of the location of the carbon site, i . Owing to this behavior, at least, the on-site interaction strength on $\phi_i(\mathbf{r})$ is concluded to be approximately the same for all the carbon sites.

The two-body effective interaction terms, *e.g.* the Hubbard interaction, are given as an operator expansion of the Coulomb scattering processes minus the mean-field counter terms.[41–44] The interacting effective Hamiltonian along the line of the Wannierization takes the form of the extended Hubbard model with N_C sites. The scattering processes in this representation should contain various off-site interactions, as well as the on-site Hubbard interaction U .

Here, if one suppose that the longer-ranged interaction is irrelevant to be neglected, and if on-site repulsion U only is kept in a general tight-binding description, the obtained Hubbard model might be less accurate for our target system. The description could be shifted from the true answer of the electronic structure in V_{111} . This is because we have a localized zero mode, in which the development of the electron correlation evolves differently from the extending quasi-particle modes in the Dirac cones. Note that the both modes, the zero mode and the quasi-particle modes, are given as combinations of $\phi_i(\mathbf{r})$. But, the former is a localized state with exponentially

decaying tails.

Rather than the usage of U on $\phi_i(\mathbf{r})$, we should classify the scattering processes into an on-site interaction U_0 on the zero-mode and the others. Both of the scattering processes include the off-site interaction in representation of the LCAO picture using $\phi_i(\mathbf{r})$. This statement is easily shown by expanding the U_0 term, which will be given in Eq. (4), into two-body effective interactions among several π orbitals, $\phi_i(\mathbf{r})$. Long-range interaction processes cannot be neglected.

Therefore, we go to the other way, starting from the band structure, or the momentum-space representation without using the Wannier transformation explicitly. Selecting only $(3n+1) \times (3n+1)$ super cells, we evaluate scattering amplitudes relevant for V_{111} . Here, we utilize the description by the multi-reference density functional theory (MR-DFT), which allows us to introduce two-body interaction terms as a quantum fluctuation

in the energy density functional.[45, 46] From now on, the creation and annihilation operators, $c_{k,\sigma}^\dagger$ and $c_{k,\sigma}$, are to be defined by the basis given by the Kohn-Sham effective single-particle Hamiltonian. The charge density, $n(\mathbf{r})$, is initially given by a local-density approximation (LDA), which is reconsidered after obtaining a solution of an effective many-body problem.

The correlation effect is counted by introducing a two-body correlation function explicitly in the energy functional. In the present situation, an important term is the next. Let us introduce a mean electron number in the zero mode, $N_0 = \langle \hat{n}_{0\uparrow} + \hat{n}_{0\downarrow} \rangle$. At the half-filling of the zero mode, $N_0 = 1$. We need to subtract a contribution from the Hartree term after consideration of the two-body term explicitly. Thus we have a kind of two-body effective Hamiltonian, $H_0^{(2)}$.

$$H_0^{(2)} = \frac{U_0}{2} \left\{ : (\hat{n}_{0\uparrow} + \hat{n}_{0\downarrow})^2 : - N_0 (\hat{n}_{0\uparrow} + \hat{n}_{0\downarrow}) \right\}. \quad (3)$$

Here : \hat{A} : represents a normal ordering of a product, \hat{A} , of the Fermion operators and the number operator is given as usual, $\hat{n}_{0\sigma} = c_{k=0,\sigma}^\dagger c_{k=0,\sigma}$. Under a condition, $N_0 = 1$, we have a corresponding interaction term appearing in the symmetric Anderson model,

$$H_0^{(2)} = U_0 \left(\hat{n}_{0\uparrow} - \frac{1}{2} \right) \left(\hat{n}_{0\downarrow} - \frac{1}{2} \right) - \frac{U_0}{4}, \quad (4)$$

providing that the total system is minimized when the local charge neutral condition, $N_0 = 1$, is kept.

One might consider a counter term coming from the exchange-correlation potential. In the discussion of V_{111} , we suppose that $N_0 = 1$ is kept by the correlation effect in a range of μ . Actually, we can find a finite parameter space of the resulting Kondo Hamiltonian, where the $N_0 = 1$ condition is kept. (See Section III B.) The correlation causes redistribution of electrons in the Dirac cone. However, it appears only as a tiny change in a momentum distribution function along the energy axis. Within a reasonable accuracy, the final charge density is

unchanged. This means that every functional of $n(\mathbf{r})$ is not shifted after inclusion of the explicit correlation effects via the short-range interaction (correlation) terms in the effective Hamiltonian. Therefore, the contribution of the DFT exchange-correlation energy is not relevant for the present argument.

The value of correlation energy U_0 in Eq. (4) is estimated by evaluating it as a partially screened Coulomb integral. We utilized the DFT-LDA simulation to have the basis for the estimation. The plane-wave expansion with the norm-conserving pseudo-potentials is adopted with the cut-off of a value from 25 to 40 Ry. After checking reasonable convergence in the estimated scattering amplitudes, we utilize the value of 25 Ry for relatively large simulation cells. The estimation results in $U_0 = 0.6, 0.6, 1.3$ eV for $7 \times 7, 10 \times 10$, and 13×13 cells, respectively. (Fig. 2) Although the value is not converging systematically, we suppose that there is a finite value of U_0 of order eV.

In addition to Eq. (4), we have many types of scattering processes promoting magnetic behavior. Owing to finiteness of U_0 , we assume $N_0 = 1$ at around the charge neutral point, *i.e.* $\mu = 0$. Among processes, we keep the spin-dependent scatterings in a form of the s - d interaction in our discussion. Similar estimation of the spin-exchange scattering with the partial screening tells us the next result.

Let us now consider amplitude $J_{kk'}$ of the spin-dependent scattering. Here the suffix k may be interpreted as a combined index of the band and the wave vector. In our formalism, however, we utilize a basis of modes defined in a selected large super cell. Therefore, k specifies a low-energy π mode. Note that the matrix element, $J_{kk'}$, represents a scattering amplitude of an electron in a mode k to another mode k' by a magnetic scattering by the zero mode spin.

As the lowest order direct exchange scattering, $J_{kk'}^{direct}$, we have always the diagonal ferromagnetic contribution, J_{kk}^{direct} . This is only because the zero mode and each Dirac mode are orthogonal with each other. The off-diagonal terms in the first order are relatively smaller than the diagonal element. Because the Dirac mode is extending wave, while the zero mode is localized, the absolute value of $J_{kk'}^{direct}$ decreases, when the super cell size increases. We have actually a scaling relation of $J_{kk'}^{direct} \sim O(1/n)$, which goes to zero in the large cell limit. Therefore, the exchange integral $J_{kk'}^{direct}$ should behave as a monotonically decreasing function of the cell size. (Fig. 2)

There is a higher-order magnetic scattering term. A typical second order contribution reads,

$$J_{kk'}^{super} = \frac{1}{2} \sum_{|\epsilon_p| > \epsilon_c} \left\{ \frac{V_{(0k) \rightarrow (0p)} V_{(0p) \rightarrow (k'0)}}{\epsilon_p - \epsilon_k} + \frac{V_{(0k) \rightarrow (p0)} V_{(p0) \rightarrow (k'0)}}{\epsilon_p - \epsilon_k} \right\}. \quad (5)$$

Here, ϵ_k denotes the single particle energy of the mode k ,

where ε_k and $\varepsilon_{k'}$ are within a cut off of ε_c , and $V_{(0k) \rightarrow (pq)}$ is a Coulomb scattering amplitude. For details of derivation, see Appendix D.

Let's suppose that we have a Born-von-Karman boundary condition for the description of the wave function of the Dirac bands of graphene. Wave functions in the Dirac cones are characterized by a wave vector around the K or K' points. When the difference of \mathbf{k} from \mathbf{k}_K (or $\mathbf{k}_{K'}$) is small, we have an asymptotic wave function, *i.e.* those of the $k \cdot p$ approximation in the Weyl representation. Introducing the envelop function, we have the long-wave length limit for the low energy excitations. In this limit, the exchange scattering within each valley should have a momentum independent amplitude.

For V_{111} , we have unbalanced sublattice structure. Therefore, the so-called chiral symmetry in the pure graphene is not used. Furthermore, we evaluate the amplitudes of two-particle scattering among modes at the Γ -point in FBZ. Therefore, k represents the band index. Namely, without using the Born-von-Karman boundary condition, we perform a size-scaling analysis. The value and the sign of $J_{kk'}^{super}$ might depend on the cell size, again.

In the large cell limit, we should have amplitudes which are almost k -independent in the low energy regime except for a degrees of freedom coming from the sublattice site index. In this limit, the form of Eq. (5) can have a non-negligible contribution owing to the integration with respect to the intermediate modes. In addition, similar to the old super-exchange mechanism, anti-ferromagnetic contribution should be dominant, because of a larger domain for the intermediate state than that for ferromagnetic processes.

Material dependence of $J_{kk'}^{super}$ comes from the sign and the magnitude of amplitude, $V_{(0k) \rightarrow (0p)}$ and $V_{(0p) \rightarrow (k'0)}$, and the spectrum ε_k . In the present case, we have relatively large contribution for the anti-ferromagnetic channel, where $V_{(0k) \rightarrow (0p)} V_{(0p) \rightarrow (k'0)}$ is positive real valued.

In our estimation, we see a systematic increase of relative contribution in the anti-ferromagnetic channels for larger cells. The order of magnitude for $J_{kk'}^{super}$ is estimated to be ~ 0.2 eV in finite cells, whose temperature scale is $O(10^3)$ K. (Fig. 2) However, the convergence is not enough achieved within an accessible cell size for the DFT simulations.

To show converging behavior of the asymptotic form of $J_{kk'}^{super}$, we combine results by the t model with the DFT estimation. (See Appendix D.) In Fig. 2, the total magnitude of J^{super} is multiplied by a factor to adjust the two values for a cell of $n = 3$. In comparison with J^{super} , the direct exchange J^{direct} is negligible in the large cell size limit.

C. Representation in a Kondo model

The effective model of V_{111} is represented by a Kondo Hamiltonian below. Here, $\epsilon_0 = \varepsilon_0 - U_0/2 - \mu$, and

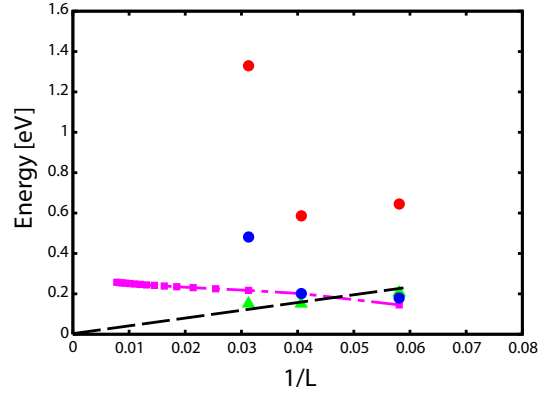


FIG. 2. Estimated interaction strength, U_0 (red dots), J^{direct} (green triangles), and J^{super} (blue dots). We adopt a $(3n + 1) \times (3n + 1)$ cell with $n = 2, 3, 4$. The length L of the super cell size is given by $L = (3n + 1)\sqrt{3}a$ [\AA] with a [\AA] be the bond length of pure graphene. For J^{direct} , the dashed line gives a guide to the eyes. The magenta squares are J^{super} estimated by the t model, whose magnitudes are multiplied by a constant, so that the data for $n = 3$ is adjusted to the DFT estimation.

$$\epsilon_k = \varepsilon_k - \mu.$$

$$H_{Kondo} = H_0 + H_J + H_D, \quad (6)$$

$$H_0 = \sum_{\sigma=\uparrow\downarrow} \epsilon_0 c_{0\sigma}^\dagger c_{0\sigma} + U_0 \hat{n}_{0\uparrow} \hat{n}_{0\downarrow},$$

$$H_J = (c_{0\sigma}^\dagger \vec{\sigma}_{\sigma\sigma'} c_{0\sigma'}) \sum_{kk'} J_{kk'} (c_{k\tau}^\dagger \vec{\sigma}_{\tau\tau'} c_{k'\tau'}),$$

$$H_D = \sum_{k,\tau} \epsilon_k c_{k\tau}^\dagger c_{k\tau}.$$

In Eqs. (6), H_0 represents the energy level of the zero mode and the on-site Coulomb repulsion U_0 on the zero mode. H_J represents the effective scattering process of conduction electrons caused by exchange interactions $J_{kk'}$ between the electrons on the zero mode and the Dirac electrons. H_D is the Hamiltonian for the Dirac electrons. σ and τ indicate the spin components of electrons on the zero mode and the Dirac electrons, respectively. Repeated indexes, σ and τ , in H_J are assumed to be summed with respect to the spin direction.

As discussed in Section II B, the simplest modeling of V_{111} incorporating the correlation effect is to have the diagonal single-body term and the off-diagonal general two-body terms. Among the two-body scatterings, the on-site interaction at the zero mode and the exchange scattering processes keeping the electron number of the zero mode are relevant for the strong correlation regime. Therefore, the above modeling is a natural model for HGV with topological zero modes.

D. Transformation to an impurity Anderson model

In order to treat the Kondo hamiltonian numerically, we transform H_{Kondo} into an effective Anderson model.[47] We can convert the form of H_J in Eqs. (6) into a separable form by diagonalizing $J_{kk'}$ with a unitary matrix as

$$\begin{aligned} H_J &= (c_{0\sigma}^\dagger \vec{\sigma}_{\sigma\sigma'} c_{0\sigma'}) \sum_{kk'} J_{kk'} (c_{k\tau}^\dagger \vec{\sigma}_{\tau\tau'} c_{k'\tau'}) \\ &= (c_{0\sigma}^\dagger \vec{\sigma}_{\sigma\sigma'} c_{0\sigma'}) \\ &\times \sum_l \left\{ \left(\sum_k c_{k\tau}^\dagger U_{J,kl} \right) \bar{J}_l \vec{\sigma}_{\tau\tau'} \left(\sum_{k'} U_{J,lk'}^{-1} c_{k'\tau'} \right) \right\} \\ &= (c_{0\sigma}^\dagger \vec{\sigma}_{\sigma\sigma'} c_{0\sigma'}) \sum_l \bar{c}_{l\tau}^\dagger \bar{J}_l \vec{\sigma}_{\tau\tau'} \bar{c}_{l\tau'}. \end{aligned} \quad (7)$$

Here, \bar{J}_l are matrix elements of the diagonalized matrix, $\bar{J} = U_J^{-1} J U_J$, and $\bar{c}_{l\tau}^\dagger$ (or $\bar{c}_{l\tau'}$) are given by $\sum_k c_{k\tau}^\dagger U_{J,kl}$ (or $\sum_{k'} U_{J,lk'}^{-1} c_{k'\tau'}$). We assume that \bar{J}_l is ordered in a descending series.

By considering the most effective $\bar{J}_{l=1}$ alone, and by obtaining \bar{H}_D by substituting $c_{k\tau}$ in an expansion with $\bar{c}_{k\tau}$ for H_D in Eqs. (6), we can transform H_{Kondo} into $H_{Anderson}$ as

$$\begin{aligned} H_{Kondo} &= H_{Anderson} + O(1/N_C), \\ H_{Anderson} &= \bar{H}_0 + \bar{H}_D + \bar{H}_{hyb}. \end{aligned} \quad (8)$$

Here, each term is given by,

$$\begin{aligned} \bar{H}_0 &= \sum_{\sigma=\uparrow\downarrow} \epsilon_0 c_{0\sigma}^\dagger c_{0\sigma} + U_0 \hat{n}_{0\uparrow} \hat{n}_{0\downarrow} \\ &+ \sum_{\sigma=\uparrow\downarrow} \epsilon'_{11} \bar{c}_{1\sigma}^\dagger \bar{c}_{1\sigma} + \bar{J}_1 (c_{0\sigma}^\dagger \vec{\sigma}_{\sigma\sigma'} c_{0\sigma'}) (\bar{c}_{1\tau}^\dagger \vec{\sigma}_{\tau\tau'} \bar{c}_{1\tau'}), \end{aligned}$$

$$\begin{aligned} \bar{H}_D &= \sum_{k \neq 1, \sigma} \epsilon'_{kk} \bar{c}_{k\sigma}^\dagger \bar{c}_{k\sigma}, \\ \bar{H}_{hyb} &= \sum_{k \neq 1, \sigma} (\epsilon'_{k1} \bar{c}_{k\sigma}^\dagger \bar{c}_{1\sigma} + H.c.). \end{aligned}$$

Note that hybridization ϵ'_{k1} as single-body parts in Eqs. (8) come from the off-diagonal elements of $\epsilon'_{kk'} = \sum_{k''} U_{J,kk''}^{-1} \epsilon_{k''} U_{J,k''k'}$.

E. The s -channel exchange term

In the transformation in Section IID, we note that there could be several \bar{J}_l s, which became non-negligible, in general. Besides, U_J does give various off-diagonal hybridization terms in addition to the diagonal term, \bar{H}_D . Let's evaluate these terms by considering an ideal case.

As discussed in Section IIB, $J_{k,k'}$ approaches to a constant asymptotically for the low-energy quasi-particle modes, when the system size becomes enough large.

Therefore, the most typical model of $J_{k,k'}$ is a matrix with constant elements.

Introducing an $n \times n$ matrix, $J = (J_{k,k'})$, as

$$J = J_0 \begin{pmatrix} 1 & 1 & \cdots & 1 \\ 1 & 1 & \cdots & 1 \\ \vdots & \vdots & \ddots & \vdots \\ 1 & 1 & \cdots & 1 \end{pmatrix}, \quad (9)$$

we see that $\bar{J}_{l=1} = nJ_0$ and $\bar{J}_{l>1} = 0$. To diagonalize J , we can choose a unitary matrix

$$U_J = \begin{pmatrix} 1/\sqrt{n} & 1/\sqrt{2} & 1/\sqrt{6} & \cdots & 1/\sqrt{n(n-1)} \\ 1/\sqrt{n} & -1/\sqrt{2} & 1/\sqrt{6} & \cdots & 1/\sqrt{n(n-1)} \\ 1/\sqrt{n} & 0 & -2/\sqrt{6} & \cdots & 1/\sqrt{n(n-1)} \\ \vdots & \vdots & \vdots & \ddots & \vdots \\ 1/\sqrt{n} & 0 & 0 & \cdots & \frac{-(n-1)}{\sqrt{n(n-1)}} \end{pmatrix}.$$

Indeed, the transformed J is,

$$U_J^{-1} J U_J = J_0 \begin{pmatrix} n & 0 & \cdots & 0 \\ 0 & 0 & \cdots & 0 \\ \vdots & \vdots & \ddots & \vdots \\ 0 & 0 & \cdots & 0 \end{pmatrix}.$$

By applying U_J , the single-particle part is transformed. Actually, the unitary transformation changes the diagonal matrix,

$$\epsilon = \begin{pmatrix} \epsilon_1 & 0 & \cdots & 0 \\ 0 & \epsilon_2 & \cdots & 0 \\ \vdots & \vdots & \ddots & \vdots \\ 0 & 0 & \cdots & \epsilon_n \end{pmatrix}$$

into

$$\epsilon' = U_J^{-1} \epsilon U_J = \begin{pmatrix} \epsilon'_{11} & \epsilon'_{12} & \cdots & \epsilon'_{1n} \\ \epsilon'_{21} & \epsilon'_{22} & \cdots & \epsilon'_{2n} \\ \vdots & \vdots & \ddots & \vdots \\ \epsilon'_{n1} & \epsilon'_{n2} & \cdots & \epsilon'_{nn} \end{pmatrix}.$$

Let us introduce another transformation to have an ideal form. Taking a $(n-1) \times (n-1)$ unitary matrix $u_{\epsilon'}$ which diagonalizes a block matrix

$$\epsilon'' = \begin{pmatrix} \epsilon'_{22} & \epsilon'_{23} & \cdots & \epsilon'_{2n} \\ \epsilon'_{32} & \epsilon'_{33} & \cdots & \epsilon'_{3n} \\ \vdots & \vdots & \ddots & \vdots \\ \epsilon'_{n2} & \epsilon'_{n3} & \cdots & \epsilon'_{nn} \end{pmatrix},$$

we can make a unitary matrix $U_{J\epsilon} = U_J U_{\epsilon}$ where

$$U_{\epsilon} = \begin{pmatrix} 1 & 0 \\ 0 & u_{\epsilon'} \end{pmatrix}.$$

The transformation by $U_{J\epsilon}$ keeps the diagonal form of the J term.

$$\begin{aligned}\tilde{J} &= U_{J\epsilon}^{-1} J U_{J\epsilon} \\ &= J_0 \begin{pmatrix} n & 0 & \cdots & 0 \\ 0 & 0 & \cdots & 0 \\ \vdots & \vdots & \ddots & \vdots \\ 0 & 0 & \cdots & 0 \end{pmatrix} = \begin{pmatrix} \tilde{J}_{l=1} & 0 & \cdots & 0 \\ 0 & 0 & \cdots & 0 \\ \vdots & \vdots & \ddots & \vdots \\ 0 & 0 & \cdots & 0 \end{pmatrix}, \quad (10)\end{aligned}$$

while the ϵ term changes its shape into a desired form as,

$$\tilde{\epsilon} = U_{J\epsilon}^{-1} \epsilon U_{J\epsilon} = \begin{pmatrix} \tilde{\epsilon}_1 & V_{21}^* & V_{31}^* & \cdots & V_{n1}^* \\ V_{21} & \tilde{\epsilon}_2 & 0 & \cdots & 0 \\ V_{31} & 0 & \tilde{\epsilon}_3 & \cdots & 0 \\ \vdots & \vdots & \vdots & \ddots & \vdots \\ V_{n1} & 0 & 0 & \cdots & \tilde{\epsilon}_n \end{pmatrix}.$$

We see that the spectrum of ϵ_i is almost reproduced by $\tilde{\epsilon}_i$, when n is enough large. Therefore, the Anderson Hamiltonian shown in Section II D represents the Kondo Hamiltonian without any essential correction, if $J_{k,k'}$ behaves as a constant among relevant quasi-particle modes.

In case when ϵ_i has degeneracy, we have additional simplification in the transformed matrices, $\tilde{\epsilon}$ and \tilde{J} . This comes from the s -wave nature of the present model interaction, H_J , with J by Eq. (9). To see this behavior, let assume that $\epsilon_i = \epsilon_m$ for $1 \leq i \leq m$. Let us consider a transformation among degenerate states by,

$$\begin{aligned}U_P &= \begin{pmatrix} U_{J,m} & 0 \\ 0 & I \end{pmatrix}, \\ U_{J,m} &= \begin{pmatrix} 1/\sqrt{m} & 1/\sqrt{2} & \cdots & 1/\sqrt{m(m-1)} \\ 1/\sqrt{m} & -1/\sqrt{2} & \cdots & 1/\sqrt{m(m-1)} \\ 1/\sqrt{m} & 0 & \cdots & 1/\sqrt{m(m-1)} \\ \vdots & \vdots & \ddots & \vdots \\ 1/\sqrt{m} & 0 & \cdots & -(m-1)/\sqrt{m(m-1)} \end{pmatrix}.\end{aligned}$$

Here I is an $(n-m) \times (n-m)$ identity matrix. Introducing another $(n-m) \times (n-m)$ matrix,

$$J_{n-m} = J_0 \begin{pmatrix} 1 & 1 & \cdots & 1 \\ 1 & 1 & \cdots & 1 \\ \vdots & \vdots & \ddots & \vdots \\ 1 & 1 & \cdots & 1 \end{pmatrix},$$

we see that,

$$U_P^{-1} J U_P = \begin{pmatrix} U_{J,m}^{-1} J_m U_{J,m} & \hat{J}_m \\ \hat{J}_m & J_{n-m} \end{pmatrix},$$

$$U_{J,m}^{-1} J_m U_{J,m} = J_0 \begin{pmatrix} m & 0 & \cdots & 0 \\ 0 & 0 & \cdots & 0 \\ \vdots & \vdots & \ddots & \vdots \\ 0 & 0 & \cdots & 0 \end{pmatrix},$$

$$\hat{J}_m = J_0 \begin{pmatrix} \sqrt{m} & \sqrt{m} & \cdots & \sqrt{m} \\ 0 & 0 & \cdots & 0 \\ \vdots & \vdots & \ddots & \vdots \\ 0 & 0 & \cdots & 0 \end{pmatrix},$$

$$U_P^{-1} \epsilon U_P = \epsilon,$$

The above result is naturally interpreted using representations of the permutation group of m elements. Namely, only the fully symmetric representation has the exchange contribution, while the other representations have zero matrix elements, as far as J is assumed to be given by Eq. (9). Keeping the symmetric representation, omitting the others in the degenerate levels, we have a reduced exchange matrix,

$$J^{red} = J_0 \begin{pmatrix} m & \sqrt{m} & \cdots & \sqrt{m} \\ \sqrt{m} & 1 & \cdots & 1 \\ \vdots & \vdots & \ddots & \vdots \\ \sqrt{m} & 1 & \cdots & 1 \end{pmatrix},$$

where J^{red} has no more constant matrix elements. Therefore, we can choose each symmetric representation created by degenerate states, which may be called states of the s symmetry, to construct the reduced exchange matrix.

When the matrix J is given as a matrix with constant elements, our Hamiltonian reads as,

$$\begin{aligned}H_{Kondo} &= H_{Anderson}, \\ H_{Anderson} &= \tilde{H}_0 + \tilde{H}_D + \tilde{H}_{hyb}.\end{aligned} \quad (11)$$

Here, each term is given by,

$$\begin{aligned}\tilde{H}_0 &= \sum_{\sigma=\uparrow\downarrow} \epsilon_0 c_{0\sigma}^\dagger c_{0\sigma} + U_0 \hat{n}_{0\uparrow} \hat{n}_{0\downarrow} \\ &+ \sum_{\sigma=\uparrow\downarrow} \tilde{\epsilon}_1 \tilde{c}_{1\sigma}^\dagger \tilde{c}_{1\sigma} + \tilde{J}_1 (c_{0\sigma}^\dagger \vec{\sigma}_{\sigma\sigma'} c_{0\sigma'}) (\tilde{c}_{1\tau}^\dagger \vec{\sigma}_{\tau\tau'} \tilde{c}_{1\tau'}), \\ \tilde{H}_D &= \sum_{k \neq 1, \sigma} \tilde{\epsilon}_k \tilde{c}_{k\sigma}^\dagger \tilde{c}_{k\sigma}, \\ \tilde{H}_{hyb} &= \sum_{k \neq 1, \sigma} (V_{k1} \tilde{c}_{k\sigma}^\dagger \tilde{c}_{1\sigma} + H.c.).\end{aligned}$$

Here, $\tilde{c}_{l\tau}^\dagger$ (or $\tilde{c}_{l\tau'}$) are given by $\sum_k c_{k\tau}^\dagger U_{J\epsilon,kl}$ (or $\sum_{k'} U_{J\epsilon,lk'}^{-1} c_{k'\tau'}$). The one-body Hamiltonian, \tilde{H}_D , describes renormalized Dirac modes with the modified spectrum, $\tilde{\epsilon}_k$.

III. CALCULATION RESULTS AND DISCUSSIONS

A. The CT-HYB-QMC method

In this section, we apply a numerical method for an impurity-problem to the Anderson Hamiltonian derived in the last section. We can trace the behavior of $H_{Anderson}$ with a continuous-time hybridization-expansion matrix solver (the CT-HYB-QMC solver) of

the quantum Monte-Carlo method. The solver is provided by the TRIQS project.[48]

A reason for the application is its powerful ability to handle the impurity problem with a few impurity sites. In addition, the QMC algorithm is useful to treat a general bath Green function. The temperature range in our concern is accessible by CT-HYB-QMC. Another reason is because the CT-HYB algorithm treats any interacting impurity model with finite interaction strength of U_0 and $J_{k,k'}$ effectively.[49, 50] We applied a transformation to the Anderson model, which allows us to apply the package with CT-HYB-QMC directly.

We regard the effective Anderson model described in Eq. (8) or Eq. (11) as a two-site impurity Anderson model (TIAM). The center orbital is the zero mode, $\phi_0(\mathbf{r})$. As a result of the transformation in Section IID, we have an additional localized orbital. Let us name an orbital, which is magnetically hybridized with the zero mode by the exchange interaction of $\tilde{J}_{l=1}$, ‘the first orbital’. As usual impurity Anderson systems, we have hybridization terms, \tilde{H}_{hyb} , which form ‘a Kondo cloud’ in the renormalized Dirac modes. We calculated the mean value of the number of electrons in ‘the first orbital’, $N_{first} = \langle \hat{n}_{1\uparrow} \rangle + \langle \hat{n}_{1\downarrow} \rangle$ where $\hat{n}_{1\sigma} = \tilde{c}_{1\sigma}^\dagger \tilde{c}_{1\sigma}$, as well as that in the zero mode, $N_{zero} = \langle \hat{n}_{0\uparrow} \rangle + \langle \hat{n}_{0\downarrow} \rangle$, to characterize the electronic state and the correlation effect in the system.

B. Calculation results

As a consequence of the unitary transformation on the Dirac modes, an energy level $\tilde{\epsilon}_1$, which is the site energy of the first orbital, appears at the Dirac point. So, we take $\epsilon_0 = -U_0/2 - \mu$ for the zero mode and $\tilde{\epsilon}_1 = -\mu$ for the first orbital in this calculation.

The density of states in the low-energy excitations of Dirac electrons are modeled by that of the t model. We adopted a value $t = 3.03[\text{eV}]$ for the nearest neighbor transfer.[51] In this section, we take the inverse temperature $\beta = 100/t = 33[1/\text{eV}]$. The interaction strength of $U_0 = 1[\text{eV}]$ is adopted.

We assume that each element $J_{k,k'}$ of the effective exchange scattering matrix $J = (J_{k,k'})$ is almost a constant among the low-energy modes in the Dirac cone, and its size $|J| = \tilde{J}_{l=1}$ is in a range estimated in Sec. IIB. Therefore, we treat $\tilde{J}_{l=1}$ as a parameter within this energy scale.

Another parameter for this modeling is the energy range of Dirac modes, for which $J_{k,k'}$ is finite. This value corresponds to the matrix size n of J . We have checked that the result is qualitatively the same irrespective of the range of Dirac modes for which V_{k1} is finite. Thus, we adopt a continuous representation of $\tilde{\epsilon}_k$ and V_{k1} , where an average, V_0 , of V_{k1} is taken for simplicity. We will discuss dependence of the main results on V_{k1} , which is assumed to be in a scale of J_0 in simulations.

The chemical potential μ changes the Fermi level in the

Dirac electrons, which affects the occupation of localized modes in turn. The chemical potential dependence of N_{first} (and N_{zero}) of the model is obtained and shown in Fig. 3.

In our model, the on-site interaction U_0 at the zero mode has enough large value of $O(\text{eV})$. Therefore, the zero mode keeps its identity as a singly occupied mode. Namely, $N_0 = N_{zero}$ is almost kept at 1, at least if $|\mu| < U/2$, where the condition of $N_0 = 1$ is necessary for the consistency as a simulation of MR-DFT. Then, an unpaired spin exists at the zero mode. The problem described by $H_{Anderson}$ is magnetic screening effect mediated by exchange interactions.

When $|J|$ is smaller than about $0.1[\text{eV}]$, N_{first} drops from 0.0 to 2.0 instantly. The result tells that electron occupation at an effective localized level, *i.e.* the first orbital, follows the un-correlated free electron behavior. This is a weak-coupling limit of the system, although U_0 keeps the half-filling of the zero mode. Therefore, when $\tilde{J}_{l=1}$ is too small against other parameters, *i.e.* the temperature and V_{k1} , we have a weak-coupling scheme without magnetic screening,

When $\tilde{J}_{l=1}$ is large enough, anti-ferromagnetic correlation evolves between the zero mode and the effective localized level, *i.e.* the first orbital. Indeed, N_{first} shows a stepwise behavior. This behavior indicates that correlation develops in the Dirac electrons. This result suggests that $J_{kk'}$ in Eqs. (6) can mediate the Kondo screening of the spin $1/2$ in the zero mode at the low temperature. The region for this screening to work has a V-shaped structure opening in the larger $|J|$ region widely against μ in the μ - $|J|$ space.

Here V_{k1} is assumed to have a value of order $0.1[\text{eV}]$. When V_{k1} is getting smaller, the graph shown in Fig. 3 becomes much sharper at the edges of the V-shaped structure. Therefore, we conclude that the physical picture given here is qualitatively kept as far as $|J|$ being finite and V_{k1} is small.

C. Strong coupling regime in the large system size limit

The physical picture of the above result may be interpreted as follows. Consider a finite anti-ferromagnetic coupling $\tilde{J}_{l=1}$. This interaction creates or defines an imaginative localized state as a linear combination of the Dirac levels. (Fig. 4) This interaction-driven localized orbital, *i.e.* the first orbital, is also half-filled, when μ is at the Dirac point. An electron in this mode and the zero-mode electron couple with the anti-ferromagnetic interaction. Owing to a finite V_{k1} , however, the screening becomes imperfect. A finite amplitude of the magnetic moment may appear at the zero mode.

In our model, thus, we have a weak coupling limit of $\tilde{J}_{l=1} = 0$ (Fig. 4 (a)) where an unscreened spin $s = 1/2$ remains at the zero mode, and a strong coupling regime shown in Fig. 4 (c) where the perfect screening happens

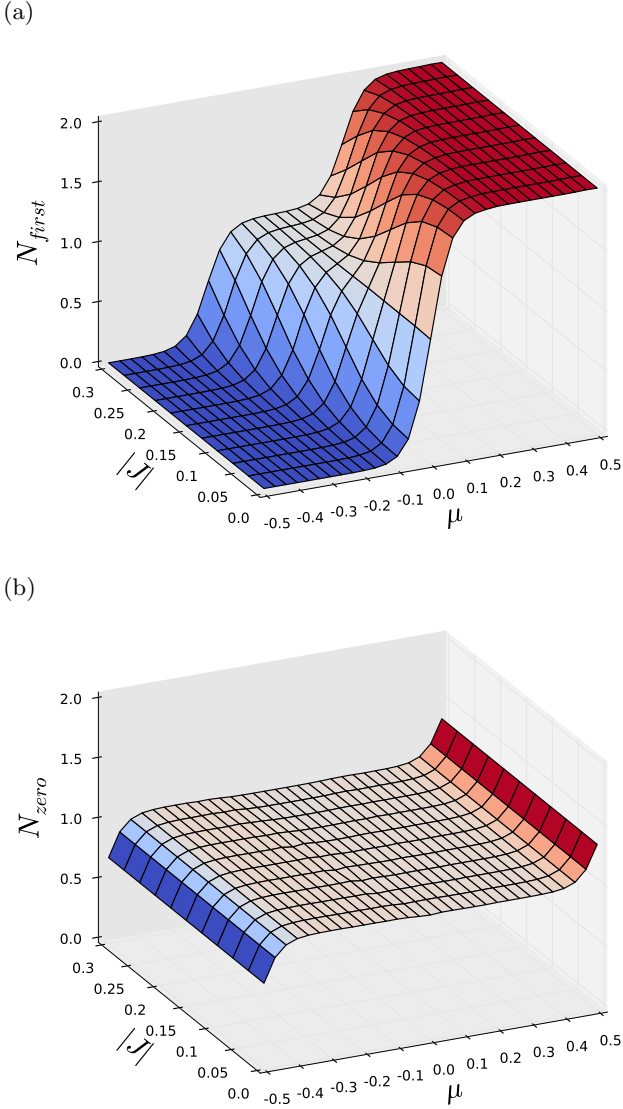


FIG. 3. (a) The number of electrons in “the first orbital”, N_{first} , and its chemical potential dependence. The chemical potential is given by μ [eV]. The exchange interaction, $|J|$, between the zero mode and the Dirac electrons is anti-ferromagnetic. We can see continuous change of N_{first} where $|J|$ is small, and stepwise change of N_{first} where $|J|$ is large. (b) The number of electrons in the zero mode, N_{zero} . When $|\mu|$ is smaller than $U_0/2 = 0.5$ [eV], $N_{zero} \simeq 1$, and the zero mode is kept at the half-filling.

as formation of a singlet pair between the zero mode and the first orbital. When the weak coupling regime is realized, we should have a free electron behavior in the Dirac modes, which is not renormalized. While, in the strong coupling regime, we should find a magnetic moment of $1\mu_B$ mainly in the Dirac mode out of the zero mode. Here we assumed that the g factor is 2 and μ_B is the Bohr magneton.

The numerical result in the last section tells that the half-filling, *i.e.* $N_{first} = 1$, is kept, even when μ is

slightly shifted around the Dirac point, if stability of the screening happens owing to finite $\tilde{J}_{l=1}$. Therefore, the large $|J|$ area in the V-shaped region is the strong-coupling regime.

At this stage, one might suspect that the present result is qualitatively different from those discussed in the pseudogap Kondo problem.[4] Often the problem is analyzed using the single-site impurity Anderson model (SIAM), where an impurity site is embedded in a pseudogapped semi-metal. Owing to the disappearing density of states at the charge neutral point, magnetic interaction mediated by the hybridization term between the impurity site and the pseudogapped metal disappears. The heuristic renormalization group approach concludes that an unscreened spin remains to keep the system with the doublet ground state. Therefore, the Kondo screening is concluded to be lost for the model at the half-filling.

In our model, since the magnetic interaction is mediated by two-body scattering terms $V_{(0,k) \rightarrow (pq)}$, the interaction strength $\tilde{J}_{l=1}$ remains to be finite. The exchange is mediated by a kind of the super exchange process, where scattering of electrons via the Coulomb interaction causes virtual processes among unoccupied Dirac modes. We can explain the existence of the process as effective perturbation processes using a discretized spectrum as illustrated in Fig. 4. On the contrary, the hybridization between the zero mode and the Dirac electrons is always zero in our modeling. Therefore, we call the mechanism “scattering-driven Kondo screening”. This picture also tells us that the large cell limit is inevitably in the strong-coupling regime, as follows.

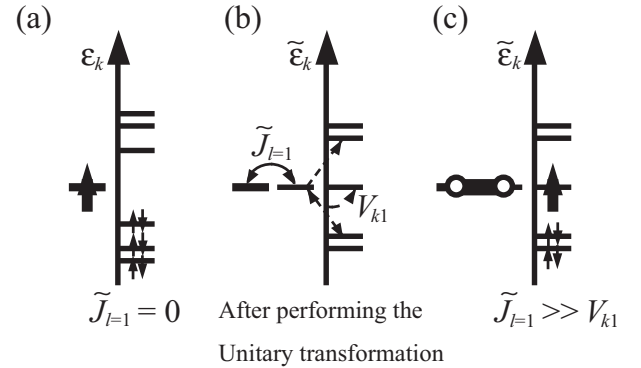


FIG. 4. Schematic viewgraph of crossover happened for scattering-driven Kondo screening. (a) A center level by the thick line represents a zero mode of V_{111} and the other levels are from the Dirac cone. When J_0 is negligible, the zero mode with $U_0 > 0$ has a single free spin. (b) The two-body scattering processes by $J_{k,k'}$ mediate the relevant super exchange J_0 , where a unitary transformation given by $J_{k,k'}$ for the metallic Dirac cone states selects the first orbital $\phi_1(\mathbf{r})$, defines renormalized spectrum $\tilde{\epsilon}_i$, and determines one-body hybridization $V_{1,k}$. (c) When $\tilde{J}_{l=1}$ is kept finite, the screening happens, while V_{21} approaches zero, if the system size increases, providing the renormalized Dirac cone.

Following the unitary transformation introduced in

Sec. IID, we have another third zero energy mode in resulted renormalized spectrum, $\tilde{\epsilon}_k$. (Fig. 4 (b)) Owing to $J_{k,k'}$, we have a local singlet within two sites of TIAM, *i.e.* the zero mode and the first orbital, in the strong coupling regime. Then, an unpaired electron appears in another zero energy mode. (Fig. 4 (c)) This crossover behavior from the weak to the strong coupling limit allows to have the doublet ground state in the whole parameter space considered. We may note that the real magnetic regime with possible higher spin states appears, only when $J_{kk'}$ behaves ferromagnetically. This can happen when J^{direct} works.

Interestingly, the super-exchange process works most effectively, when only a few Dirac modes around the Fermi level come close to the zero mode energetically. This condition is also met at the half filling.

As noted, the hybridization term, \tilde{H}_{hyb} , is determined by ϵ_k . When the system size grows, two low-lying Dirac states around the Dirac point approach to zero. In this limit, V_{21} goes to zero. Then, by taking the large size limit, no matter small $\tilde{J}_{l=1}$ is, as far as $J_{l=1}$ is finite, we have a strong coupling regime for the large system size.

The remaining Dirac electrons are, at the same time, renormalized in its spectrum, *i.e.* from ϵ_k to $\tilde{\epsilon}_k$. The number of the modes in $\tilde{\epsilon}_k$ is reduced by one from that of ϵ_k . Then, even though the free electron picture of the Dirac cone gives an even-numbered spectrum of ϵ_k , the renormalized Dirac band has another zero-energy mode decoupled from the zero mode in the strong correlation regime. Thus, we have a renormalized Dirac-cone state in TIAM, which is different from a semi-metallic state in an unscreened regime of SIAM.

When μ is changed by the order of $\tilde{J}_{l=1}$, the half-filling nature of the extra localized mode, *i.e.* $N_{first} = 1$, is lost as shown in Fig. 3 (a). However, even when the magnetic screening disappears, the strong on-site interaction U_0 of the zero mode may keep the localized spin 1/2 at the center of V_{111} . (Fig. 3 (b)) Therefore, around the Dirac point, we may tune the local magnetic property of V_{111} only by changing the charge donation condition. As well-known, the gate bias can control μ rather easily for the graphene device structure.

IV. CONCLUSIONS

In conclusion, we derived a model for the zero mode of the hydrogenated atomic vacancy of graphene, V_{111} . The model is given by a Kondo Hamiltonian, where the two-particle scattering processes produce anti-ferromagnetic super exchange between the zero mode spin and low-lying modes of the Dirac cones. By way of a unitary transformation, we introduced a two-site impurity Anderson Hamiltonian, by which we traced the behavior of the model with continuous-time quantum Monte-Carlo calculation. The calculation results of the model suggests that the spin 1/2 on the zero mode on the V_{111} structure may be magnetically screened by the Dirac electrons at

low temperatures.

Since the total system is a Kramers doublet at the half-filling, the remaining electron occupies the renormalized Dirac spectrum of odd numbered modes. In our many-body representation, however, the renormalized Dirac cones keeps its nature as a zero-gap semiconductor.

Our result strongly suggests an interesting behavior of V_{111} , which had been created in a gate-biased graphene channel of electronic devices. The present simulation tells that the zero mode appears at the Dirac point, whose spectrum at around the V_{111} structure can be controlled qualitatively by the filling control. Behavior of the spin 1/2 can be easily controlled by the external charge donation in the graphene variants.

In this paper, we focused on V_{111} . In this structure, a single zero mode appears at the band center. When the electron (or hole) doping in the host graphene becomes large enough to create the Fermi surface structure, the electron-hole symmetry is broken. The Friedel oscillation in graphene[52, 53] would then be determined by a way reconstructing a self-consistent charge distribution, $n(\mathbf{r})$. When a secondary order parameter in magnetism grows at the same time, our multi-reference density functional theory requires to determine the four current density as a source of the internal electro-magnetic field. A magnetic phase created by the RKKY interaction would, then, be determined in a self-consistent way.

The description adopted in this paper takes several approximations *a priori*. This is because we looked at a many-body effect caused by “a pure zero mode” of graphene. People have already derived enhanced spin-orbit coupling driven by the σ - π mixing at a hydrogen impurity,[54–56] whose signal in nature was reported.[57] When we introduce an effective single-particle Hamiltonian taking the spin-orbit coupling into account, the Kondo-type magnetic screening effect derived in this paper might explain a reason for the seemingly weak spin scattering by a localized electron in the zero mode. Furthermore, magnetic field direction dependence of the electron spin resonance and detection of photo induced quantum oscillation would complete our understanding of the impurity state experimentally.

Our strategy of modeling is, however, hold for a wider class of defects of graphene, or pseudogapped Kondo systems. Analysis of graphene vacancy and atom-adsorbed graphene, as well as direct comparison with the experiments will be discussed elsewhere, by which nature of correlation effects in the zero mode of Dirac spectrum shall be further explored.

ACKNOWLEDGMENTS

The authors greatly thank stimulating discussions and fruitful comments by Dr. M. Ziatdinov, Dr. Y. Kudo, Prof. S. Fujii, Prof. M. Kiguchi, and Prof. T. Mori. They also appreciate helpful comments by Dr. H. Ueda. The calculations were partly done in the com-

puter centers of Research Center for Information Technology, Kyushu University and Institute for Solid State Physics, University of Tokyo. This work is supported by the Grand-in-Aid for scientific research (No. 235404080, No. 26107526, and No. 26400357) from MEXT, Japan.

Appendix A: Bandstructure results by DFT-LDA

We show band structures of V_{111} in two super cells given by the LDA calculations. The Born-von Karman boundary condition is adopted. Fig. 5 is for the 6×6 cell, and Fig. 6 is for the 7×7 cell. The density of states of the former structure is shown in Fig. 7.

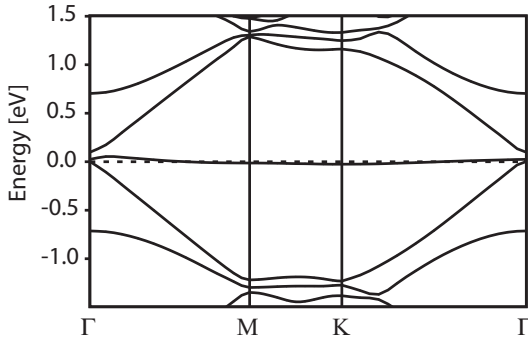


FIG. 5. The LDA band structure of V_{111} in a 6×6 super cell.

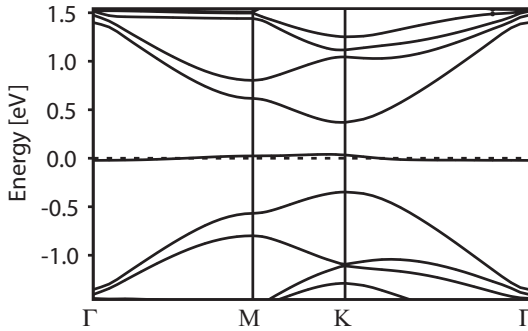


FIG. 6. The LDA band structure of V_{111} in a 7×7 super cell.

The size scaling of some relevant energies in the band structure is shown in Fig. 8. Here, only $(3n+1) \times (3n+1)$ super cells are considered. In the limit of $L \rightarrow \infty$, the energy of the bottom of the flat band given by the blue line points an energy slightly below the gap closing point of the Dirac modes. By counting the electron correlation effect, however, our effective many-body model keeps the zero mode as a half-filled localized orbital.

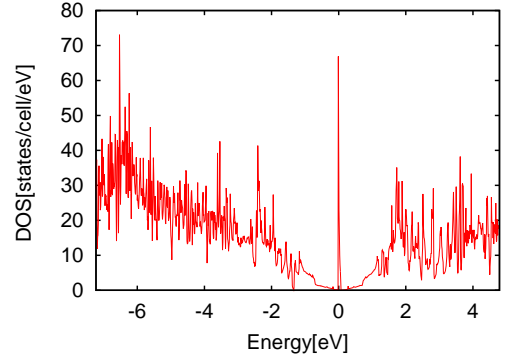


FIG. 7. The LDA density of states for V_{111} in a 6×6 super cell.

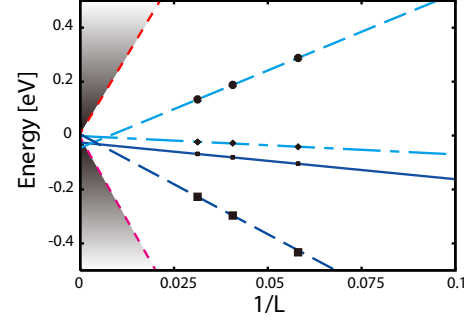


FIG. 8. Scaling relation of relevant energy for a $(3n+1) \times (3n+1)$ series of the supercells. The band bottom and the band top of the flat band (BBFB and BTFB) are given by the data connected by the solid line and the dot-dashed line. The shaded areas represent the energy range of the Dirac modes at the Γ point in each super cell with the side-length L . The gap by the vacancy creation approaches to zero in the limit of $L \rightarrow \infty$. The dashed lines are the top (or bottom) of the Dirac branch appearing at the K (or K') points in FBZ of the super cell.

Appendix B: A definition of a π orbital on a deformed graphene

For the deformed graphene, we are able to define a π network only by geometry of the atomic structure within a linear combination of atomic orbital (LCAO) scheme.

The direction of a σ bond of a carbon atom is given by either local C-C or C-H direction. We have three direction vectors $\mathbf{a}_j^i = (a_{1j}^i, a_{2j}^i, a_{3j}^i)$ with $j = 1, 2, 3$ for the i -th carbon atom. These vectors determine three σ -like orbitals, where each hybridized σ wave function is given by

$$\psi_{\sigma,j}^i(\mathbf{r}) = C_{2s,j}^i \phi_{2s}^i(\mathbf{r}) + \sum_{k=1,2,3} C_{2p,k,j}^i \phi_{2p,k}^i(\mathbf{r}), \quad (\text{B1})$$

where an index $k = 1, 2, 3$ corresponding to x, y, z . Here, $\phi_{2s}^i(\mathbf{r})$ and $\phi_{2p,k}^i(\mathbf{r})$ are the local atomic orbital in a spatially fixed Cartesian coordinate. The coefficients are

given by

$$C_{2s,j}^i = \frac{1}{C_j^i} \sqrt{\frac{|\mathbf{a}_{j'}^i \cdot \mathbf{a}_j^i| |\mathbf{a}_{j''}^i \cdot \mathbf{a}_j^i|}{|\mathbf{a}_{j'}^i \cdot \mathbf{a}_{j''}^i|}}, \quad (\text{B2})$$

$$C_{2p,k,j}^i = \frac{1}{C_j^i} a_{kj}^i, \quad (\text{B3})$$

$$C_j^i = \sqrt{\frac{|\mathbf{a}_{j'}^i \cdot \mathbf{a}_j^i| |\mathbf{a}_{j''}^i \cdot \mathbf{a}_j^i|}{|\mathbf{a}_{j'}^i \cdot \mathbf{a}_{j''}^i|} + \sum_{k=1,2,3} (a_{kj}^i)^2}. \quad (\text{B4})$$

Here j , j' , and j'' are mutually different. Note that, for sp^2 -like hybridization, where the relative angle between two different direction vectors \mathbf{a}_j^i and $\mathbf{a}_{j'}^i$ are almost $2\pi/3$, the inner product $\mathbf{a}_j^i \cdot \mathbf{a}_{j'}^i$ is negative valued.

Now, we have a unique local π wave function,

$$\psi_\pi^i(\mathbf{r}) = D_{2s}^i \phi_{2s}^i(\mathbf{r}) + \sum_{k=1,2,3} D_{2p,k}^i \phi_{2p,k}^i(\mathbf{r}), \quad (\text{B5})$$

on each carbon atom, where $\psi_\pi^i(\mathbf{r})$ is orthogonal to three $\psi_{\sigma,j}^i(\mathbf{r})$. Thus, the coefficients, $(D_{2s}^i, D_{2p,k}^i)$, are determined uniquely except for a global phase factor, so that it is normalized and orthogonal to $(C_{2s,j}^i, C_{2p,k}^i)$ with $k = 1, 2, 3$. We have also $1s$ orbitals $\phi_{1s}^l(\mathbf{r})$ for three hydrogen atoms ($l = 1, 2, 3$).

Using this definition of the π orbital, we can introduce a topological mapping from the t model to another tight-binding model in LCAO of σ and π orbitals. The dimension of a subspace given by $\{\psi_\pi^i\}$ is N_C , while that of LCAO is $4N_C + 3$. Therefore, we have a submatrix of the LCAO Hamiltonian to be compared with H_{TBM} in Eq. (2). In a deformed structure, we have a finite transfer term from σ to π orbital, as well as a long range transfer term. The mapping from the second model to the t model is defined as continuous reduction in both the σ - π hybridization and the long-range π - π transfer.

Appendix C: Mappings between zero modes for $3n \times 3n$ supercells

If one is required to consider another series of $3n \times 3n$, we may i) introduce an effective magnetic flux to change the gauge along an in-plane direction, ii) choose a Γ point only calculation to have an effective band gap, and iii) apply evaluation in the same manner as discussed below. When we see a convergence of the obtained effective model for $n \rightarrow \infty$, the description in the thermodynamic limit is achieved.

If one requires direct identification of the zero mode in $3n \times 3n$ super cells, there is another way, which is realized by incorporating two Wannier transformations. The zero mode, $\phi_0(\mathbf{r})$, may be given by adopting the Wannier transformation of the center flat band. This is always possible, since there is an energy window required for the definition. (Fig. 5) By the second Wannier transformation of the whole π bands, we have defined

π orbitals $\phi_i(\mathbf{r})$ for V_{111} . The set of $S_\pi = \{\phi_i(\mathbf{r})\}$ is a complete set of the π bands, by which the zero mode, $\phi_0(\mathbf{r})$, is well expanded. There is a way to derive a non-orthogonal basis of $\{\phi_0, \{\phi_l\}\}$, where we may choose $(N_C - 1)$ orbitals, $\phi_l(\mathbf{r})$, from S_π . By applying an orthogonalization method, we can have an orthogonalized set of $S'_\pi = \{\phi_0, \{\tilde{\phi}_l\}\}$. Then, we have a unitary transformation connecting S_π to S'_π . Utilizing the transformation, we can construct a Kondo Hamiltonian written in the basis of S'_π .

Appendix D: Super exchange mechanism for the zero mode

In this appendix, we introduce an intuitive method to derive a super exchange process between the zero mode and a low-lying Dirac mode. For the purpose, considering the spectrum, ε_k for the k -th Dirac mode, owing to the correlation effect, we assume that the electron occupation is one for the lowest $k = \pm 1$ modes, and that the zero mode is singly occupied. The half electron occupation in the $k = 1$ mode and a hole in the $k = -1$ mode can emerge naturally in a correlated state.

We consider a state with a singlet pair,

$$|\Psi_1\rangle = \frac{1}{\sqrt{2}}(c_{0\uparrow}^\dagger c_{k=1\downarrow}^\dagger - c_{0\downarrow}^\dagger c_{k=1\uparrow}^\dagger)|\tilde{0}\rangle. \quad (\text{D1})$$

Here the state $|\tilde{0}\rangle$ denotes a filled Dirac sea for $k < -1$ with an up electron occupying the lowest $k = -1$ mode.

$$|\tilde{0}\rangle = c_{k=-1,\uparrow}^\dagger \prod_{k < -1} c_{k,\uparrow}^\dagger c_{k,\downarrow}^\dagger |0\rangle. \quad (\text{D2})$$

For the present purpose, we may select an up state of a doublet without loss of generality. In our description, the empty modes of $k > 1$ and the filled modes of $k < -1$, which are empty hole states, contribute to produce intermediate virtual states in the super exchange processes.

Since the effective one-body Hamiltonian is diagonalized, the virtual state is created by the effective two-body Hamiltonian, which appears as the quantum fluctuation. Since the zero mode with large U_0 is in the strong correlation regime, the occupation of the zero mode does hardly fluctuate even in the virtual state. Therefore, a relevant process happens via the correlated hopping $\hat{H}_{(0k) \rightarrow (0p)}^{ch}$ and the exchange hopping $\hat{H}_{(0k) \rightarrow (p0)}^{eh}$. We consider an effective Hamiltonian for these processes,

$$\begin{aligned} \hat{H}_{(0k) \rightarrow (0p)}^{ch} &= V_{(0k) \rightarrow (0p)} \left(c_{0,\uparrow}^\dagger c_{p,\downarrow}^\dagger c_{k,\downarrow} c_{0,\uparrow} + c_{p,\uparrow}^\dagger c_{0,\downarrow}^\dagger c_{0,\downarrow} c_{k,\uparrow} \right), \\ \hat{H}_{(0k) \rightarrow (p0)}^{eh} &= V_{(0k) \rightarrow (p0)} \left(c_{p,\uparrow}^\dagger c_{0,\downarrow}^\dagger c_{k,\downarrow} c_{0,\uparrow} + c_{0,\uparrow}^\dagger c_{p,\downarrow}^\dagger c_{0,\downarrow} c_{k,\uparrow} \right). \end{aligned}$$

When $p > k$, the action of the effective two-particle

Hamiltonian is,

$$\begin{aligned} & (\hat{H}_{(01) \rightarrow (0p)}^{ch} + \hat{H}_{(01) \rightarrow (p0)}^{eh}) |\Psi_1\rangle \\ &= (V_{(0k) \rightarrow (0p)} + V_{(0k) \rightarrow (p0)}) \frac{1}{\sqrt{2}} (c_{0\uparrow}^\dagger c_{p\downarrow}^\dagger - c_{0\downarrow}^\dagger c_{p\uparrow}^\dagger) |\tilde{0}\rangle. \end{aligned}$$

As an intermediate state owing to the quantum fluctuation, a singlet is formed between the singly-occupied p mode and the zero mode. For comparison, let us also test a triplet state.

$$|\Psi_2\rangle = \frac{1}{\sqrt{2}} (c_{0\uparrow}^\dagger c_{k=1\downarrow}^\dagger + c_{0\downarrow}^\dagger c_{k=1\uparrow}^\dagger) |\tilde{0}\rangle, \quad (D3)$$

which behaves as,

$$\begin{aligned} & (\hat{H}_{(01) \rightarrow (0p)}^{ch} + \hat{H}_{(01) \rightarrow (p0)}^{eh}) |\Psi_2\rangle \\ &= (V_{(0k) \rightarrow (0p)} - V_{(0k) \rightarrow (p0)}) \frac{1}{\sqrt{2}} (c_{0\uparrow}^\dagger c_{p\downarrow}^\dagger + c_{0\downarrow}^\dagger c_{p\uparrow}^\dagger) |\tilde{0}\rangle. \end{aligned}$$

These are processes by quasi-electron excitation. (Fig. 9 (a)) There are other processes by quasi-hole excitation, where a filled $k = 1$ state and a hole at a mode with $p < -1$ appear. (Fig. 9 (b))

Using these results, we can readily obtain the expression of the super exchange energy mediated by the intermediate states with ϵ_p as an energy difference between two states, $|\Psi_1\rangle$ and $|\Psi_2\rangle$.

$$\begin{aligned} & \Delta E(\Psi_2) - \Delta E(\Psi_1) \\ &= \sum_{|\epsilon_p| > \epsilon_{k=1}} \frac{2(V_{(0k) \rightarrow (0p)} V_{(0p) \rightarrow (k0)} + V_{(0k) \rightarrow (p0)} V_{(p0) \rightarrow (k0)})}{\epsilon_p - \epsilon_{k=1}}. \end{aligned}$$

The final form of the super exchange interaction between the zero mode and a k mode has the next form as a scattering of the electron at the k mode to another k' mode.

$$\hat{H}_{kk'}^{super} = J_{kk'}^{super} (c_{0\sigma}^\dagger \vec{\sigma}_{\sigma\sigma'} c_{0\sigma'}) \cdot (c_{k\tau}^\dagger \vec{\sigma}_{\tau\tau'} c_{k'\tau'}), \quad (D4)$$

with

$$\begin{aligned} J_{kk'}^{super} &= \frac{1}{2} \sum_{|\epsilon_p| > \epsilon_c} \left\{ \frac{V_{(0k) \rightarrow (0p)} V_{(0p) \rightarrow (k'0)}}{\epsilon_p - \epsilon_k} \right. \\ &\quad \left. + \frac{V_{(0k) \rightarrow (p0)} V_{(p0) \rightarrow (k'0)}}{\epsilon_p - \epsilon_k} \right\}. \end{aligned} \quad (D5)$$

Here ϵ_c is a cut off to separate the low-energy phase space active for the exchange scattering and higher energy virtual states. In a finite size system, we may choose only the lowest excitation of $k = \pm 1$ for the low-energy modes. While we see quasi-degeneracy at the $k = 1$ (or $k = -1$) mode often in a super cell result. Therefore, we keep an expression with the cutoff energy.

Relevant information on the estimation of $J_{kk'}^{super}$ is the next. One might suspect that the exchange hopping amplitudes, $V_{(0k) \rightarrow (p0)}$, might not be enough large to have a finite value of $J_{kk'}^{super}$. We have tested overlap of the

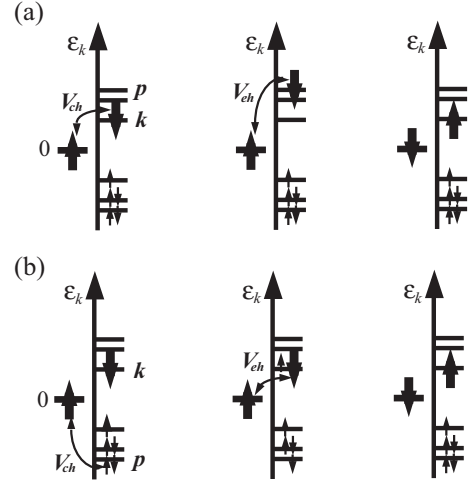


FIG. 9. Super-exchange processes in (a) an electron channel and (b) a hole channel for the zero mode $k = 0$. The electron in a mode k interacts with the localized electron at the zero mode via the correlated hopping V_{ch} to make a virtual state. The exchange hopping V_{eh} exchanges two spins, which completes the super exchange.

wave function of the t model. Let's introduce eigen states and eigen functions of the t model. In this appendix, we omit the spin index in each expression for simplicity.

$$\hat{H}_{TBM} |\psi_k\rangle = \tilde{\epsilon}_k |\psi_k\rangle, \quad (D6)$$

$$|\psi_k\rangle = \sum_i \psi_{k,i} C_i^\dagger |0\rangle, \quad (D7)$$

$$\psi_k(\mathbf{r}) = \sum_i \psi_{k,i} \phi_i(\mathbf{r}), \quad (D8)$$

$$\int d^3r \phi_i^*(\mathbf{r}) \phi_j(\mathbf{r}) = \delta_{ij}. \quad (D9)$$

The last equality is the orthogonality among the Wannier orbitals. A next integral is estimated.

$$\begin{aligned} & \tilde{V}_{(0k) \rightarrow (p0)} \\ &= \frac{e^2}{2} \iint d^3r d^3r' \frac{\psi_p^*(\mathbf{r}) \psi_0^*(\mathbf{r}') \psi_k(\mathbf{r}') \psi_0(\mathbf{r})}{|\mathbf{r} - \mathbf{r}'|} \\ &= \frac{e^2}{2} \sum_{i_1, i_2, i_3, i_4} \psi_{p,i_1}^* \psi_{0,i_2}^* \psi_{k,i_3} \psi_{0,i_4} \tilde{v}_{i_1, i_2, i_3, i_4}, \end{aligned} \quad (D10)$$

$$\begin{aligned} & \tilde{v}_{i_1, i_2, i_3, i_4} \\ &= \iint d^3r d^3r' \frac{\phi_{i_1}^*(\mathbf{r}) \phi_{i_2}^*(\mathbf{r}') \phi_{i_3}(\mathbf{r}') \phi_{i_4}(\mathbf{r})}{|\mathbf{r} - \mathbf{r}'|}. \end{aligned} \quad (D11)$$

Using an approximate expression $\tilde{v}_{i_1, i_2, i_3, i_4} = \tilde{v}(|\mathbf{R}_{i_1} - \mathbf{R}_{i_2}|) \delta_{i_1, i_4} \delta_{i_2, i_3}$ with the position of the i -th carbon atom, \mathbf{R}_i , and

$$\tilde{v}(|\mathbf{R}_{i_1} - \mathbf{R}_{i_2}|) = \begin{cases} v_0 & \text{for } \mathbf{R}_{i_1} = \mathbf{R}_{i_2} \\ \frac{v_0}{|\mathbf{R}_{i_1} - \mathbf{R}_{i_2}|} & \text{for } \mathbf{R}_{i_1} \neq \mathbf{R}_{i_2} \end{cases},$$

we may evaluate asymptotic behavior of $\tilde{V}_{(0k) \rightarrow (p0)}$ as well as $\tilde{V}_{(0k) \rightarrow (0p)}$ for a large super cell. In this estima-

tion, however, we cannot determine the absolute value of the integral, or v_0 , since $\phi_i(\mathbf{r})$ is not explicitly given. Therefore, we choose a finite system to adjust J^{super} in this evaluation to the value by the DFT result. The result is shown in Fig. 2 of the main text.

Using the estimation by the t model, we can derive another key. Let us show the local density of states around V_{111} . (Fig. 10) In the A -sites neighboring to the vacancy, we have a clear indication of the zero mode as a sharp peak of LDOS at the center of the spectrum. We see a clear enhancement of LDOS at the $A-1$ site, even when the energy is rather in the Dirac spectrum. We have also a slight signal of enhancement at the $A-2$ site. This result suggests us that local overlap between a low-lying Dirac electron and the zero mode electron around V_{111} . Owing to this overlap of the wave function, we have non-negligible contribution $\tilde{V}_{(0k) \rightarrow (p0)}$ as well as $\tilde{V}_{(0k) \rightarrow (0p)}$.

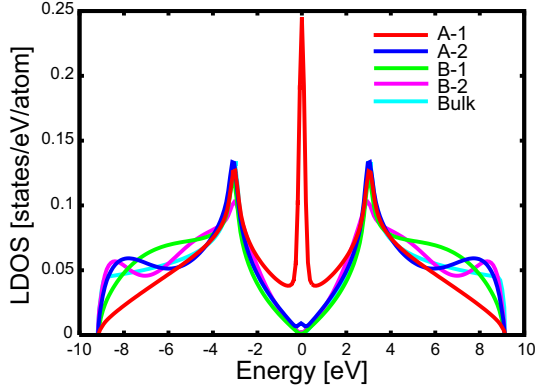


FIG. 10. The local density of states (LDOS) of the V_{111} structure. The value is estimated by the t model with the 100×100 super cell. Each lines depict LDOS at the first carbon site in the A sub-lattice ($A-1$), the nearest neighbor B -site ($B-1$), the second nearest A -site ($A-2$), the third nearest B -site ($B-2$), and a site apart from the vacancy (Bulk).

-
- [1] A. H. Castro Neto, F. Guinea, N. M. R. Peres, K. S. Novoselov, and A. K. Geim. The electronic properties of graphene. *Rev. Mod. Phys.*, 81:109–162, Jan 2009.
 - [2] K. S. Novoselov, A. K. Geim, S. V. Morozov, D. Jiang, Y. Zhang, S. V. Dubonos, I. V. Grigorieva, and A. A. Firsov. Electric field effect in atomically thin carbon films. *Science*, 306:666, 2004.
 - [3] K. S. Novoselov, A. K. Geim, S. V. Morozov, D. Jiang, M. I. Katsnelson, I. V. Grigorieva, S. V. Dubonos, and A. A. Firsov. Two-dimensional gas of massless dirac fermions in graphene. *Nature (London)*, 438:197, 2005.
 - [4] Lars Fritz and Matthias Vojta. The physics of kondo impurities in graphene. *Reports on Progress in Physics*, 76(3):032501, 2013.
 - [5] Vitor M. Pereira, F. Guinea, J. M. B. Lopes dos Santos, N. M. R. Peres, and A. H. Castro Neto. Disorder induced localized states in graphene. *Phys. Rev. Lett.*, 96:036801, Jan 2006.
 - [6] P. Haase, S. Fuchs, T. Pruschke, H. Ochoa, and F. Guinea. Magnetic moments and kondo effect near vacancies and resonant scatterers in graphene. *Phys. Rev. B*, 83:241408, Jun 2011.
 - [7] Elizabeth Duplock, Matthias Scheffler, and Philip Lindan. Hallmark of perfect graphene. *Phys. Rev. Lett.*, 92:225502, Jun 2004.
 - [8] D. Jacob and G. Kotliar. Orbital selective and tunable kondo effect of magnetic adatoms on graphene: Correlated electronic structure calculations. *Phys. Rev. B*, 82:085423, Aug 2010.
 - [9] Bruno Uchoa, Valeri Kotov, N. Peres, and A. Castro Neto. Localized magnetic states in graphene. *Phys. Rev. Lett.*, 101:026805, Jul 2008.
 - [10] P. Cornaglia, Gonzalo Usaj, and C. Balseiro. Localized spins on graphene. *Phys. Rev. Lett.*, 102:046801, Jan 2009.
 - [11] Bruno Uchoa, Ling Yang, S.-W. Tsai, N. Peres, and A. Castro Neto. Theory of scanning tunneling spectroscopy of magnetic adatoms in graphene. *Phys. Rev. Lett.*, 103:206804, Nov 2009.
 - [12] Bruno Uchoa, T. Rappoport, and A. Castro Neto. Kondo quantum criticality of magnetic adatoms in graphene. *Phys. Rev. Lett.*, 106:016801, Jan 2011.
 - [13] J. Sofo, Gonzalo Usaj, P. Cornaglia, A. Suarez, A. Hernández-Nieves, and C. Balseiro. Magnetic structure of hydrogen-induced defects on graphene. *Phys. Rev. B*, 85:115405, Mar 2012.
 - [14] Lin Li, Yang-Yang Ni, Yin Zhong, Tie-Feng Fang, and Hong-Gang Luo. The kondo effect of an adatom in graphene and its scanning tunneling spectroscopy. *New Journal of Physics*, 15(5):053018, 2013.
 - [15] Martina Hentschel and Francisco Guinea. Orthogonality catastrophe and kondo effect in graphene. *Phys. Rev. B*,

- 76:115407, Sep 2007.
- [16] K. Sengupta and G. Baskaran. Tuning kondo physics in graphene with gate voltage. *Phys. Rev. B*, 77:045417, Jan 2008.
 - [17] M. Ugeda, I. Brihuega, F. Guinea, and J. Gómez-Rodríguez. Missing atom as a source of carbon magnetism. *Phys. Rev. Lett.*, 104:096804, Mar 2010.
 - [18] Takahiro Kondo, Yujiro Honma, Junepyo Oh, Takahiro Machida, and Junji Nakamura. Edge states propagating from a defect of graphite: Scanning tunneling spectroscopy measurements. *Phys. Rev. B*, 82:153414, Oct 2010.
 - [19] R. R. Nair, M. Sepioni, I-L. Tsai, O. Lehtinen, J. Keinonen, A. V. Krasheninnikov, T. Thomson, A. K. Geim, and I. V. Grigorieva. Spin-half paramagnetism in graphene induced by point defects. *Nat. Phys.*, 8:199, 2012.
 - [20] Kathleen McCreary, Adrian Swartz, Wei Han, Jaroslav Fabian, and Roland Kawakami. Magnetic moment formation in graphene detected by scattering of pure spin currents. *Phys. Rev. Lett.*, 109:186604, Nov 2012.
 - [21] Jian-Hao Chen, Liang Li, William G. Cullen, Ellen D. Williams, and Michael S. Fuhrer. Tunable kondo effect in graphene with defects. *Nature Physics*, 7(7):535–538, apr 2011.
 - [22] Taro Kanao, Hiroyasu Matsuura, and Masao Ogata. Theory of defect-induced kondo effect in graphene: Numerical renormalization group study. *Journal of the Physical Society of Japan*, 81(6):063709, 2012.
 - [23] M. A. Cazalilla, A. Iucci, F. Guinea, and A. H. Castro Neto. Local Moment Formation and Kondo Effect in Defective Graphene. *ArXiv:1207.3135*, July 2012.
 - [24] Andrew K. Mitchell and Lars Fritz. Kondo effect with diverging hybridization: Possible realization in graphene with vacancies. *Phys. Rev. B*, 88:075104, Aug 2013.
 - [25] P. Lehtinen, A. Foster, Yuchen Ma, A. Krasheninnikov, and R. Nieminen. Irradiation-induced magnetism in graphite: A density functional study. *Phys. Rev. Lett.*, 93:187202, Oct 2004.
 - [26] Oleg Yazyev and Lothar Helm. Defect-induced magnetism in graphene. *Phys. Rev. B*, 75:125408, Mar 2007.
 - [27] J. J. Palacios and F. Ynduráin. Critical analysis of vacancy-induced magnetism in monolayer and bilayer graphene. *Phys. Rev. B*, 85:245443, Jun 2012.
 - [28] Maxim Ziatdinov, Shintaro Fujii, Koichi Kusakabe, Manabu Kiguchi, Takehiko Mori, and Toshiaki Enoki. Direct imaging of monovacancy-hydrogen complexes in a single graphitic layer. *Phys. Rev. B*, 89:155405, Apr 2014.
 - [29] Maxim Ziatdinov, Shintaro Fujii, Koichi Kusakabe, Manabu Kiguchi, Takehiko Mori, and Toshiaki Enoki. Visualization of electronic states on atomically smooth graphitic edges with different types of hydrogen termination. *Phys. Rev. B*, 87:115427, Mar 2013.
 - [30] C. Zener. Interaction between the d shells in the transition metals. *Phys. Rev.*, 81:440–444, Feb 1951.
 - [31] Jun Kondo. Resistance minimum in dilute magnetic alloys. *Prog. Theor. Phys.*, 32:37, 1964.
 - [32] W. Kohn and L. J. Sham. Self-consistent equations including exchange and correlation effects. *Phys. Rev.*, 140:A1133–A1138, Nov 1965.
 - [33] Anton Kokalj. Computer graphics and graphical user interfaces as tools in simulations of matter at the atomic scale. *Computational Materials Science*, 28(2):155 – 168, 2003. Proceedings of the Symposium on Software Development for Process and Materials Design.
 - [34] Elliott H. Lieb. Two theorems on the hubbard model. *Phys. Rev. Lett.*, 62:1201–1204, Mar 1989.
 - [35] D. Papaconstantopoulos, M. Mehl, S. Erwin, and M. Pederson. Tight-binding approach to computational materials science. In P. E. A. Turchi, A. Gonis, and L. Colombo, editors, *MRS Symposia Proceedings*, volume 491, page 221. Materials Research Society (Pittsburgh), 1998.
 - [36] Yousuke Kobayashi, Ken-ichi Fukui, Toshiaki Enoki, Koichi Kusakabe, and Yutaka Kaburagi. Observation of zigzag and armchair edges of graphite using scanning tunneling microscopy and spectroscopy. *Phys. Rev. B*, 71:193406, May 2005.
 - [37] P. Hohenberg and W. Kohn. Inhomogeneous electron gas. *Phys. Rev.*, 136:B864–B871, Nov 1964.
 - [38] Nicola Marzari and David Vanderbilt. Maximally localized generalized wannier functions for composite energy bands. *Phys. Rev. B*, 56:12847–12865, Nov 1997.
 - [39] Ivo Souza, Nicola Marzari, and David Vanderbilt. Maximally localized wannier functions for entangled energy bands. *Phys. Rev. B*, 65:035109, Dec 2001.
 - [40] A. A. Mostofi, J. R. Yates, Y.-S. Lee, I. Souza, D. Vanderbilt, and N. Marzari. Wannier90: A tool for obtaining maximally-localised wannier functions. *Comput. Phys. Commun.*, 178:685, 2008.
 - [41] J. Hubbard. Electron correlations in narrow energy bands. *Proc. Roy. Soc. London*, 276:238, 1963.
 - [42] J. Hubbard. Electron correlations in narrow energy bands ii. the degenerate band case. *Proc. Roy. Soc. London*, 277:237, 1964.
 - [43] J. Hubbard. Electron correlations in narrow energy bands iii. an improved solution. *Proc. Roy. Soc. London*, 281:401, 1964.
 - [44] Vladimir I. Anisimov, Jan Zaanen, and Ole K. Andersen. Band theory and mott insulators: Hubbard u instead of stoner i . *Phys. Rev. B*, 44:943–954, Jul 1991.
 - [45] K. Kusakabe. A rigorous extension of the kohn-sham equation for strongly correlated electron systems. *J. Phys. Soc. Jpn.*, 70:2038, 2001.
 - [46] K. Kusakabe, N. Suzuki, S. Yamanaka, and K. Yamaguchi. A self-consistent first-principles calculation scheme for correlated electron systems. *J. Phys. Condens. Matter*, 19:445009, 2007.
 - [47] P. W. Anderson. Localized magnetic states in metals. *Phys. Rev.*, 124:41–53, Oct 1961.
 - [48] O. Parcollet and M. Ferrero. a toolbox for research on interacting quantum systems (triqs). <http://ipht.cea.fr/triqs/>, 2011.
 - [49] Philipp Werner, Armin Comanac, Luca de’ Medici, Matthias Troyer, and Andrew J. Millis. Continuous-time solver for quantum impurity models. *Phys. Rev. Lett.*, 97:076405, Aug 2006.
 - [50] Philipp Werner and Andrew J. Millis. Hybridization expansion impurity solver: General formulation and application to kondo lattice and two-orbital models. *Phys. Rev. B*, 74:155107, Oct 2006.
 - [51] Riichiro Saito, Mitsutaka Fujita, G. Dresselhaus, and M. S. Dresselhaus. Electronic structure of graphene tubules based on c_{60} . *Phys. Rev. B*, 46:1804–1811, Jul 1992.
 - [52] Ádám Bácsi and Attila Virosztek. Local density of states and friedel oscillations in graphene. *Phys. Rev. B*, 82:193405, Nov 2010.
 - [53] J. Lawlor, S. Power, and M. Ferreira. Friedel oscillations

- in graphene: Sublattice asymmetry in doping. *Phys. Rev. B*, 88:205416, Nov 2013.
- [54] A. Castro Neto and F. Guinea. Impurity-induced spin-orbit coupling in graphene. *Phys. Rev. Lett.*, 103:026804, Jul 2009.
- [55] H. Ochoa, A. Castro Neto, and F. Guinea. Elliot-yafet mechanism in graphene. *Phys. Rev. Lett.*, 108:206808, May 2012.
- [56] Martin Gmitra, Denis Kochan, and Jaroslav Fabian. Spin-orbit coupling in hydrogenated graphene. *Phys. Rev. Lett.*, 110:246602, Jun 2013.
- [57] Jayakumar Balakrishnan, Gavin Kok Wai Koon, Manu Jaiswal, A. H. Castro Neto, and Barbaros Özyilmaz. Colossal enhancement of spin-orbit coupling in weakly hydrogenated graphene. *Nature Physics*, 9(5):284–287, mar 2013.